What is the best triangulation approach for a structured light system?

Jhacson Meza[a], Raul Vargas[a], Lenny A. Romero[b], Song Zhang[c], and Andres G. Marrugo[a]

[a]Facultad de Ingenieria, Universidad Tecnologica de Bolivar, Cartagena, Colombia
[b]Facultad de Ciencias Basicas, Universidad Tecnologica de Bolivar, Cartagena, Colombia
[c]School of Mechanical Engineering, Purdue University, West Lafayette, IN 47906, USA

ABSTRACT

It has become customary to calibrate a camera-projector pair in a structured light (SL) system as a stereo-vision setup. The 3D reconstruction is carried out by triangulation from the detected point at the camera sensor and its correspondence at the projector DMD. There are several formulations to obtain the coordinates of the 3D point, especially in the presence of noise. However, it is not clear what is the best triangulation approach. In this study, we aimed to determine the most suitable triangulation method for SL systems in terms of accuracy and execution time. We assess different strategies in which both coordinates in the projector are known (point-point correspondence) and the case in which only the one coordinate in the DMD is known (point-line correspondence). We also introduce the idea of estimating the second projector coordinate with epipolar constraints. We carried out simulations and experiments to evaluate the differences between the triangulation methods, considering the phase-depth sensitivity of the system. Our results show that under suboptimal phase-depth sensitivity conditions, the triangulation method does influence the overall accuracy. Therefore, the system should be arranged for optimal phase-depth sensitivity so that any triangulation method ensures the same accuracy.

Keywords: Fringe projection profilometry, 3D shape measurement, calibration.

1. INTRODUCTION

The calibration of a 3D structured light (SL) system is the single-most-important aspect when converting from phase to x, y, z Cartesian coordinates .[1] In general, there are two approaches for calibrating an SL system: 1) the reference-plane approach,[2] or 2) the stereo-vision method.[3] The former breaks down in non-telecentric systems due to the effects of magnification. In contrast, the latter is used more often due to its flexibility and ease of calibration.[4]

In the stereo-vision method, the camera and the projector are modeled using the pinhole model, which has been used in the computer vision community for several decades.[5] However, there is a unique aspect of SL systems compared to passive stereo systems: the phase-depth sensitivity. It has been shown that the geometry of the SL setup and the orientation of the projected fringes play an essential role in achieving maximum phase-depth sensitivity.[6–8] Therefore, the triangulation of a point $\mathbf{X}$ in space depends on solving a system of equations to obtain its 3D coordinates. However, there are several ways to solve the triangulation problem. Hence, we ask if all of these methods lead to the same result. Alternatively, how can we interpret differences in the triangulation results from different methods?

In the following sections, we briefly explain the theory behind triangulation in SL systems using the stereo-vision method, the different triangulation methods, and the experiments we conducted to test the differences in the methods. Encouraging preliminary results show that there are, in fact, differences in the results of the triangulation methods related to the phase-depth sensitivity of an SL system. In the following, we show these results and our discussion.

Further author information: (Send correspondence to A.G.M.)
A.G.M.: E-mail: agmarrugo@utb.edu.co

2. THEORY

2.1 Stereo Vision Calibration

In the stereo-vision model, the camera-projector system is considered as a binocular framework by regarding the projector as the inverse of a camera.[3] Considering a homogeneous 3D point $\mathbf{X} = [X^{\mathrm{w}}, Y^{\mathrm{w}}, Z^{\mathrm{w}}, 1]^{\mathsf{T}}$ in the world coordinate system, we find its corresponding coordinate $\mathbf{x}^c = [u^c, v^c, 1]^{\mathsf{T}}$ in the camera and $\mathbf{x}^p = [u^p, v^p, 1]^{\mathsf{T}}$ in the projector system using the following equations,

$$s^c \mathbf{x}^c = \mathbf{K}^c \, \mathbf{M}^c_{\mathrm{w}} \, \mathbf{X}^{\mathrm{w}} \ , \tag{1}$$

$$s^p \mathbf{x}^p = \mathbf{K}^p \, \mathbf{M}^p_{\mathrm{w}} \, \mathbf{X}^{\mathrm{w}} \ , \tag{2}$$

where s^c and s^p are scaling factors,

$$\mathbf{K}^c = \begin{bmatrix} f^c_u & 0 & c^c_u \\ 0 & f^c_v & c^c_v \\ 0 & 0 & 1 \end{bmatrix} \ , \quad \mathbf{K}^p = \begin{bmatrix} f^p_u & 0 & c^p_u \\ 0 & f^p_v & c^p_v \\ 0 & 0 & 1 \end{bmatrix} \ , \tag{3}$$

are the intrinsic matrices, where f_u and f_v denote the effective focal lengths along u and v directions; (c_u, c_v) is the coordinate of the principal point, and the superscripts ^{c} and ^{p} denote the parameters corresponding to the camera and projector, respectively. The matrices $\mathbf{M}^c_{\mathrm{w}}$ and $\mathbf{M}^p_{\mathrm{w}}$ represent a rigid transformation from the world coordinate system to the camera and the projector frames, respectively. Usually, the world frame is aligned with the camera frame and the transformation matrices $\mathbf{M}^c_{\mathrm{w}}$ and $\mathbf{M}^p_{\mathrm{w}}$ are defined as

$$\mathbf{M}^c_{\mathrm{w}} = \begin{bmatrix} 1 & 0 & 0 & 0 \\ 0 & 1 & 0 & 0 \\ 0 & 0 & 1 & 0 \end{bmatrix} \ , \tag{4}$$

and

$$\mathbf{M}^p_{\mathrm{w}} = \mathbf{M}^p_c = [\mathbf{R} \ \ \mathbf{t}], \tag{5}$$

where $\mathbf{M}^p_c$ is a transformation matrix from camera to projector coordinate system, composed of a rotation matrix $\mathbf{R}$ and a translation vector $\mathbf{t}$. It is also usual to define $\mathbf{P}^c = \mathbf{K}^c \, \mathbf{M}^c_{\mathrm{w}}$ as the camera projection matrix, and $\mathbf{P}^p = \mathbf{K}^p \, \mathbf{M}^p_{\mathrm{w}}$ as the projector projection matrix, where both of them are 4×4 matrices.

2.2 Lens Distortion

The presence of lens distortions of the SL system generate inaccuracies in the 3D reconstruction.[9–11] In practice, the camera and projector lenses have nonlinear distortions, which can be modeled as

$$\begin{bmatrix} u_d \\ v_d \end{bmatrix} = (1 + k_1 r^2 + k_2 r^4 + k_3 r^6) \begin{bmatrix} \bar{u} \\ \bar{v} \end{bmatrix} + \begin{bmatrix} 2p_1 \bar{u}\bar{v} + p_2(r^2 + 2\bar{u}^2) \\ 2p_2 \bar{u}\bar{v} + p_1(r^2 + 2\bar{v}^2) \end{bmatrix} \tag{6}$$

with

$$r^2 = \bar{u}^2 + \bar{v}^2 \ , \tag{7}$$

where $[k_1, k_2, k_3]$ are the radial distortion coefficients and $[p_1, p_2]$ are the tangential distortion parameters. $[u_d, v_d]^{\mathsf{T}}$ refer to the distorted points, and $[\bar{u}, \bar{v}]^{\mathsf{T}}$ are the normalized coordinates which can be calculated as

$$\begin{bmatrix} \bar{u} \\ \bar{v} \\ 1 \end{bmatrix} = \mathbf{K}^{-1} \begin{bmatrix} u \\ v \\ 1 \end{bmatrix} \ . \tag{8}$$

2.3 Phase-Depth Sensitivity

In recent years, many works have been carried out to obtain systems with higher performance and greater accuracy by optimizing the projected patterns or by optimizing the calibration parameters involved in the SL systems.[12–15] One of the most important parameters to improve the system performance is the phase-depth sensitivity, which is mainly affected by the geometry of the system and the direction and shape of the projected fringe patterns.

Wang and Zhang[6] developed an experimental procedure to obtain a fringe projection angle to increase the system's sensitivity. The fringe pattern may be rotated digitally or physically by adjusting the geometry of the system. Later, Zhou *et al.*,[7] showed mathematically that for a camera-projector configuration, the highest sensitivity of the system is achieved when the direction of the fringes is perpendicular to the camera-projector baseline. Furthermore, Zhang *et al.*[8] analyzed the sensitivity of the system along the observation field with fringe patterns of different directions using epipolar geometry, finding that the sensitivity of the system in each pixel depends on the angle between the fringe direction and the epipolar line. The best sensitivity is achieved when the fringes and the epipolar line form an angle of 90°, so that the optimal fringe pattern should be circular and centered on the epipole.

3. METHOD

The most used triangulation approach is the plane-line triangulation method.[3] In this method, we use both u^c and v^c camera coordinates (equivalent to a line in 3D space) and one coordinate in the projector, either u^p or v^p (equivalent to a plane in 3D space). In the computer vision literature, there are more triangulation strategies available for stereo-vision systems. The homogeneous (DLT), inhomogeneous, and optimal methods, are line-line triangulation approaches discussed in more detail in Ref. 5.

Here, we compare the traditional plane-line triangulation approach, with the line-line methods available in the literature, in terms of accuracy and execution time. We also consider lens distortion correction in both camera and projector. Note that both u and v coordinates are needed in the distortion model given by Eq. (6). The camera points can always be compensated for lens distortion. However, for the projector points, we need to project in both u and v directions. This limitation can be a problem in high-speed applications where typically patterns are only projected in one direction. Thus, we introduce the idea to estimate the second coordinate in the projector by using epipolar constraints with the epipolar line.

As a result, we evaluate the triangulation methods under three scenarios. 1) Projecting in both directions to obtain u^p and v^p, as shown in Fig. 1(a). This procedure allows for correcting lens distortions in the projector. 2) The most common scenario where we have only u^p or v^p in the projector by projecting in one direction. This scenario only allows us to use the plane-line triangulation approach and no lens distortions correction in the projector. 3) Here we measure one projector coordinate by projecting in one direction, and the other is estimated with the epipolar line. An example is shown in Fig. 1(b) where vertical patterns are projected, allowing us to estimate the u^p coordinate. The v^p coordinate is estimated by calculating the intersection between the phase line and the epipolar line. Hence, we can correct the projector lens distortions, and use the line-line methods in addition to the plane-line method.

3.1 Triangulation methods

We consider four triangulation methods: Plane-line, Homogeneous (DLT), Inhomogeneous, and Optimal triangulation. The plane-line only requires the (u^c, v^c) and u^p or v^p coordinates. The DLT, inhomogeneous and optimal require both (u^c, v^c) and (u^p, v^p) coordinates.

3.1.1 Plane-line method

For this approach, we solve for a 3D point $\tilde{\mathbf{X}}$ in Euclidean coordinates, and we only need a 2D coordinate from the projector. The 3D point is estimated with the following system

$$\begin{bmatrix} P^c_{31}u^c - P^c_{11} & P^c_{32}u^c - P^c_{12} & P^c_{33}u^c - P^c_{13} \\ P^c_{31}v^c - P^c_{21} & P^c_{32}v^c - P^c_{22} & P^c_{33}v^c - P^c_{23} \\ P^p_{31}u^p - P^p_{11} & P^p_{32}u^p - P^p_{12} & P^p_{33}u^p - P^p_{13} \end{bmatrix} \begin{bmatrix} X \\ Y \\ Z \end{bmatrix} = \begin{bmatrix} P^c_{14} - P^c_{34}u^c \\ P^c_{24} - P^c_{34}v^c \\ P^p_{14} - P^p_{34}u^p \end{bmatrix} , \tag{9}$$

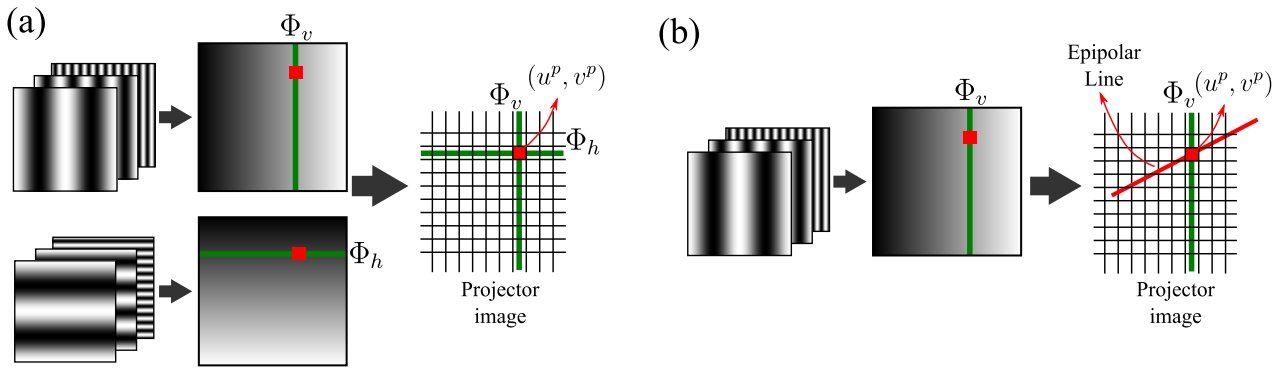

Figure 1. The two options to obtain the projector coordinates for triangulation and lens distortion correction. (a) By projecting vertical and horizontal fringes and mapping the phase values to pixel values. (b) By projecting fringes in one direction and finding the point as the intersection between the phase line and the epipolar line.

where we have three equations and three unknowns. Eq. (9) is an example of solving the system with the u^p coordinates. Moreover, because we only need one projector coordinate, this method is equivalent to a plane-line triangulation, as shown in Fig. 2(a).

This system can be solved through matrix inverse, where for N 3D points, we have to solve N times Eq. (9) making this process time-consuming. But unlike the above, because we have the same number of unknowns and equations, we can use a closed-form solution to this problem

$$X = Z\bar{u}^c \ , \tag{10}$$

$$Y = Z\bar{v}^c \ , \tag{11}$$

$$Z = \frac{t_x - t_z\bar{u}^p}{(r_{31}\bar{u}^p - r_{11})\bar{u}^c + (r_{32}\bar{u}^p - r_{12})\bar{v}^c + (r_{33}\bar{u}^p - r_{13})} \ , \tag{12}$$

where $\bar{u}^c$ and $\bar{v}^c$ are the normalized camera coordinates, and $\bar{u}^p$ is the normalized projector u^p coordinate, which can be estimated with the inverse of the intrinsic matrix as in Eq. (8). In this way, for N 3D points, we can use vector operations to find the solution faster than the matrix inverse approach.

3.1.2 Homogeneous (DLT) method

The DLT method is the triangulation approach implemented in the OpenCV library. In this method, we solve for a 3D point $\mathbf{X}$ in a homogeneous space using both u^p and v^p coordinates, as shown in Fig. 2(b). Here we have a system of four unknowns and four equations,

$$\begin{bmatrix} P^c_{31}u^c - P^c_{11} & P^c_{32}u^c - P^c_{12} & P^c_{33}u^c - P^c_{13} & P^c_{34}u^c - P^c_{14} \\ P^c_{31}v^c - P^c_{21} & P^c_{32}v^c - P^c_{22} & P^c_{33}v^c - P^c_{23} & P^c_{34}v^c - P^c_{24} \\ P^p_{31}u^p - P^p_{11} & P^p_{32}u^p - P^p_{12} & P^p_{33}u^p - P^p_{13} & P^p_{34}u^p - P^p_{14} \\ P^p_{31}v^p - P^p_{21} & P^p_{32}v^p - P^p_{22} & P^p_{33}v^p - P^p_{23} & P^p_{34}v^p - P^p_{24} \end{bmatrix} \begin{bmatrix} X_1 \\ X_2 \\ X_3 \\ X_4 \end{bmatrix} = \begin{bmatrix} 0 \\ 0 \\ 0 \\ 0 \end{bmatrix} \ , \tag{13}$$

and the solution $\mathbf{X}$ can be estimated through singular value decomposition (SVD) under the condition $||\mathbf{X}|| = 1$. Thus, for N 3D points, we need to solve N times the Eq. 13.

3.1.3 Inhomogenous method

For this method (Fig. 2(c)), we solve for an inhomogeneous 3D point $\tilde{\mathbf{X}}$ in the Euclidean space. We need both u^p and v^p coordinates, and we find the solution with the system

$$\begin{bmatrix} P^c_{31}u^c - P^c_{11} & P^c_{32}u^c - P^c_{12} & P^c_{33}u^c - P^c_{13} \\ P^c_{31}v^c - P^c_{21} & P^c_{32}v^c - P^c_{22} & P^c_{33}v^c - P^c_{23} \\ P^p_{31}u^p - P^p_{11} & P^p_{32}u^p - P^p_{12} & P^p_{33}u^p - P^p_{13} \\ P^p_{31}v^p - P^p_{21} & P^p_{32}v^p - P^p_{22} & P^p_{33}v^p - P^p_{23} \end{bmatrix} \begin{bmatrix} X \\ Y \\ Z \end{bmatrix} = \begin{bmatrix} P^c_{14} - P^c_{34}u^c \\ P^c_{24} - P^c_{34}v^c \\ P^p_{14} - P^p_{34}u^p \\ P^p_{24} - P^p_{34}v^p \end{bmatrix} \ , \tag{14}$$

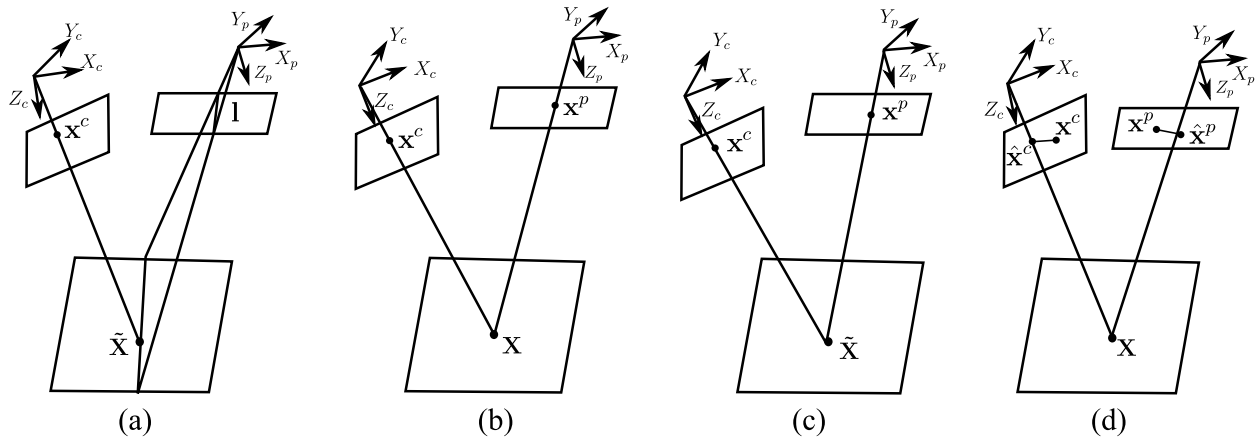

Figure 2. The four evaluated triangulation methods. (a) Plane-line. (b) Homogeneous (DLT). (c) Inhomogeneous. (d) Optimal triangulation.

where there are three unknowns and four equations. In this method, we need to estimate a least-square solution, which can be calculated with the matrix pseudoinverse, and this implies that for N 3D points, we need to solve N times the Eq. (14).

3.1.4 Optimal method

Unlike the previous methods, the optimal triangulation method is a non-linear triangulation approach robust to noisy correspondences that do not satisfy the epipolar constraint. In this strategy, we enforce the epipolar constraint between camera-projector matches with the cost function

$$C(\hat{\mathbf{x}}^c, \hat{\mathbf{x}}^p) = \|\mathbf{x}^c - \hat{\mathbf{x}}^c\|^2 + \|\mathbf{x}^p - \hat{\mathbf{x}}^p\|^2 , \text{ subject to } \hat{\mathbf{x}}^{p\mathsf{T}}\mathbf{F}\hat{\mathbf{x}}^c = 0 , \tag{15}$$

where $\hat{\mathbf{x}}^c$ and $\hat{\mathbf{x}}^p$ are close to the measured points $\mathbf{x}^c$ and $\mathbf{x}^p$ as is shown in Fig. 2(d), and they satisfy the epipolar constraint $\hat{\mathbf{x}}^{p\mathsf{T}}\mathbf{F}\hat{\mathbf{x}}^c = 0$ exactly.

After optimization, we can triangulate using the optimized matches and any linear triangulation approach (the three previously discussed methods). In this work, we combined the optimized correspondences with the DLT triangulation. Furthermore, note that this strategy has a high computational complexity because we need to find a solution to the cost function for each pair of 2D points.

3.2 Simulations and experiments

We evaluate the different triangulation methods via simulations and experiments, considering the three scenarios described above. We also consider the influence of phase-depth sensitivity on the triangulation methods.

For the simulations, we measured an ideal plane with the camera and the projector. We evaluated each method's accuracy with the RMS deviation of the point cloud to the least-squares fitted plane. Moreover, we included lens distortions. To establish the camera-projector matches, we calculate a 3D point given by the intersection between the back-projected line of each camera pixel and the ideal plane, as shown in Fig. 3. Afterward, these 3D points are projected into the projector sensor, and we add white Gaussian noise to the 2D image coordinates. Therefore, we have pixel-subpixel correspondence pairs as in an experimental camera-projector setup.

For the experiments, we evaluated the triangulation methods using the same RMS metric as in the simulations. We used two geometric configurations: 1) a suboptimal configuration, and 2) an optimal configuration. Configuration 1 is a typical camera-projector setup that is not set at the maximum phase-depth sensitivity. Configuration 2 is a phase-depth sensitivity optimized camera-projector setup, where we obtain high phase-depth sensitivity by projecting along the main projection axis, and it has a poor sensitivity by projecting patterns in the other direction.

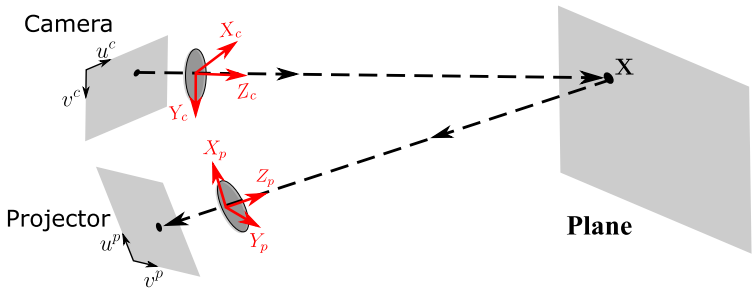

Figure 3. Procedure for establishing correspondences in the simulations. The 3D point of the intersection between the back-projected line and the ideal plane is projected onto the projector image plane and white Gaussian noise is added to it.

4. RESULTS

4.1 Triangulation error and phase-sensitivity analysis

We carried out a simulation experiment to evaluate the relation between phase-depth sensitivity and the RMS deviation under the different triangulation methods. As the sensitivity is related to the phase projection angle, to simulate the fringe angle, we rotate the projector system around the (Z-axis) optical axis, as in Ref. 7. Thus, for the same plane, we estimate each method's RMS value for each fringe angle. The results are shown in Fig. 4.

The conventional approach, where we measure one coordinate and triangulate with the plane-line method, gives the worst results. It is expected because we cannot correct for the projector lens distortions without estimating the other coordinate. Note that, unlike the previous case where we only use one projector coordinate (the solid magenta line), there are no differences between the triangulation methods when the projection angle is close to the direction of maximum sensitivity (near 0°). Conversely, when the projection angle is far from the maximum sensitivity direction, there are noticeable differences between the triangulation methods.

The plot also shows that all the line-line triangulation methods have similar performance when measuring both projector coordinates. A similar performance also occurs with the line-line methods in the case of measuring one coordinate and estimating the other. There are no differences between the DLT, the inhomogeneous, and

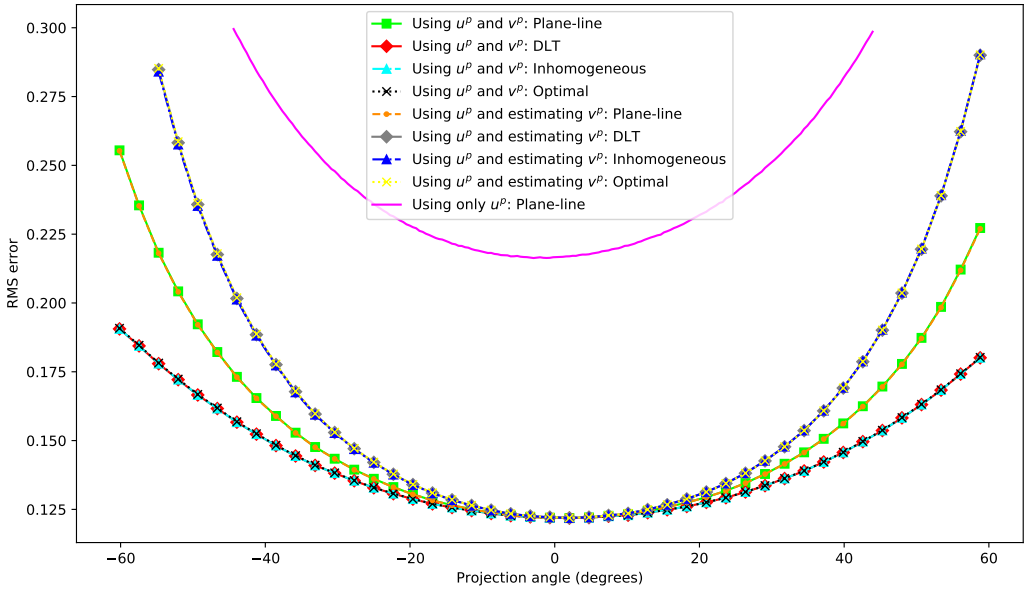

Figure 4. Simulation results of phase-sensitivity and triangulation method error analysis. There are no differences between the triangulation methods when the projection angle is close to the direction of maximum sensitivity (near 0°).

the optimal triangulation methods. Something similar occurs for the plane-line triangulation when measuring both u^p and v^p, and when measuring one direction and estimating the other with the epipolar line. We obtain the best results in the scenario where we measure both projector coordinates and triangulate with a line-line method. The second-best performance is obtained by triangulating with the plane-line method, regardless of measuring both coordinates or measuring one and estimating the other. Triangulating with the line-line methods by measuring one coordinate and estimating the other, gives us the third-best performance.

4.2 Experimental results

For the experiments, we used the two configurations previously described. In both systems, we measure a plane in five different poses to evaluate the triangulation methods under the three scenarios by projecting vertical and horizontal patterns. The RMS error results for one of the poses from configuration 1 are shown in Table 1. We can see a similar behavior to Fig. 4. Note that in this configuration, the angle between the main projection direction and the baseline is 10.97°, that is, the system is 10.97° far from the optimal projection direction. As we expected measuring only the u^p coordinate gives poor results. When measuring u^p and v^p coordinates, the results agree with the simulations, where the plane-line method gives slightly worse results. The last case where we measure u^p by projecting vertical patterns and estimate the v^p coordinates with the epipolar line, the results also agree with the simulations.

Method	**Using u^p and v^p**	**Using only u^p**	**Using u^p and estimating v^p**
Plane-line	**0.261421**	0.438151	**0.260987**
DLT	0.245759	-	0.271300
Inhomogeneous	0.246052	-	0.271082
Optimal	0.245738	-	0.271348

Table 1. Experimental RMS results of a plane pose with configuration 1.

In Fig. 5, we plotted the RMS values obtained from each reconstructed plane under the three scenarios and using the four compared methods. The line-line methods using u^p and v^p give better results with the lower RMS values. The plane-line method using u^p and v^p, and using u^p and estimating v^p with the epipolar line, gives the second-best results. The third-best results are obtained with the line-line methods using u^p and estimating v^p. This behavior is the same as in the simulation results shown in Fig. 4.

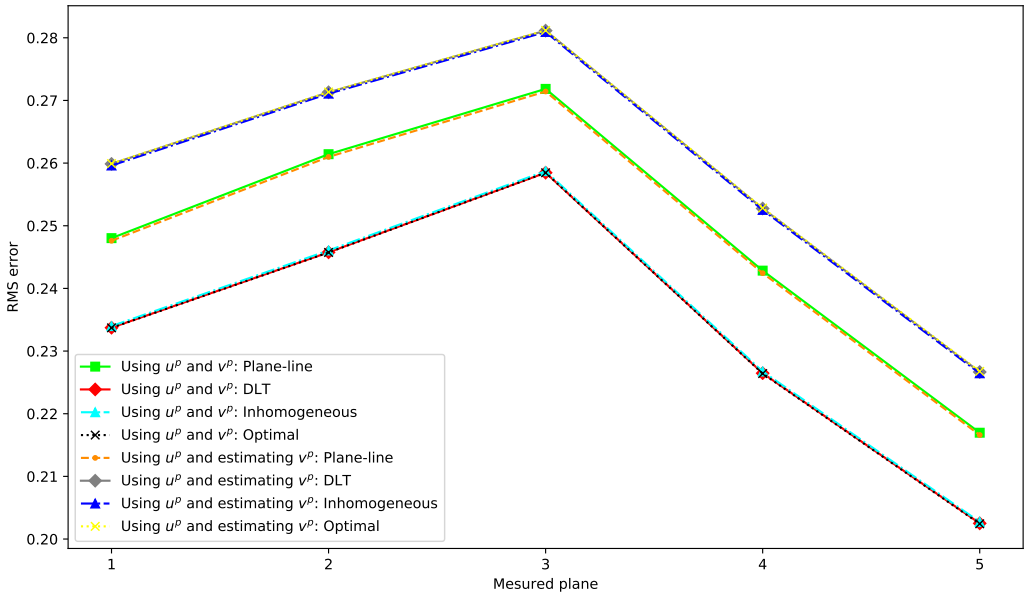

Figure 5. Experimental results of the five measured planes with configuration 1.

For configuration 2, the RMS results for one of the poses of the measured plane are shown in Table 2. We see that the differences between the triangulation methods are even closer than configuration 1. This result is because this configuration is optimized in terms of phase-depth sensitivity. The angle between the main projection axis and the projector-camera baseline is 3.25°, i.e., the main projection axis is closer to the baseline than configuration 1.

Method	**Using u^p and v^p**	**Using only u^p**	**Using u^p and estimating v^p**
Plane-line	0.225723	0.461107	0.226448
DLT	0.222843	-	0.222954
Inhomogeneous	0.222861	-	0.223520
Optimal	0.222788	-	0.222812

Table 2. Experimental RMS results of a plane pose with configuration 2.

The RMS results for all the poses are shown in Fig. 6. As expected from the simulations, the differences between the methods are smaller than the results from configuration 1. This behavior agrees with the simulation results, where near the optimal projection direction, the difference between the methods becomes negligible.

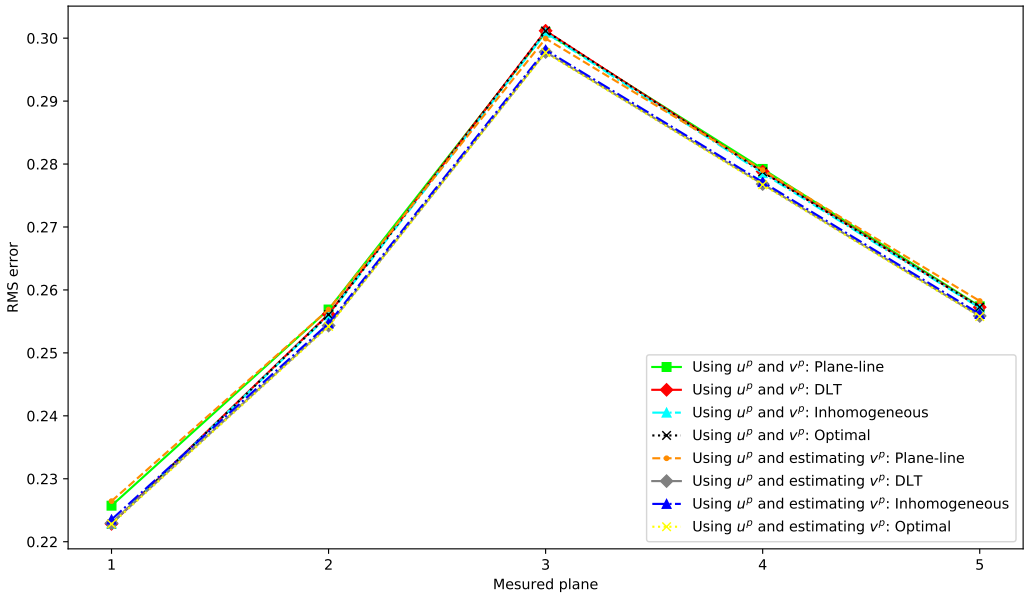

Figure 6. Experimental results of the five measured planes with configuration 2.

4.3 Time execution assessment

To evaluate the run time execution of each method, we reconstructed a total of 1310720 points 10 times with each triangulation approach. These points are from an experimental plane measured by projecting vertical and horizontal patterns. The average time for each run is shown in Fig. 7. The plane-line method outperforms the line-line methods because of the closed-form solution available with this method. The plane-line mean execution time is 0.5515 s. The mean execution time of the DLT and the Inhomogeneous methods are very similar, but the DLT method is slightly faster. The optimal method takes much longer compared to the other methods because of the additional minimization procedure.

5. CONCLUSION

In this work, we showed that although the phase-depth sensitivity plays a significant role in the accuracy of an SL system, the triangulation method also influences the overall accuracy. In general, triangulating by measuring both projector coordinates and using a line-line method, along with correcting for lens distortions, ensures the

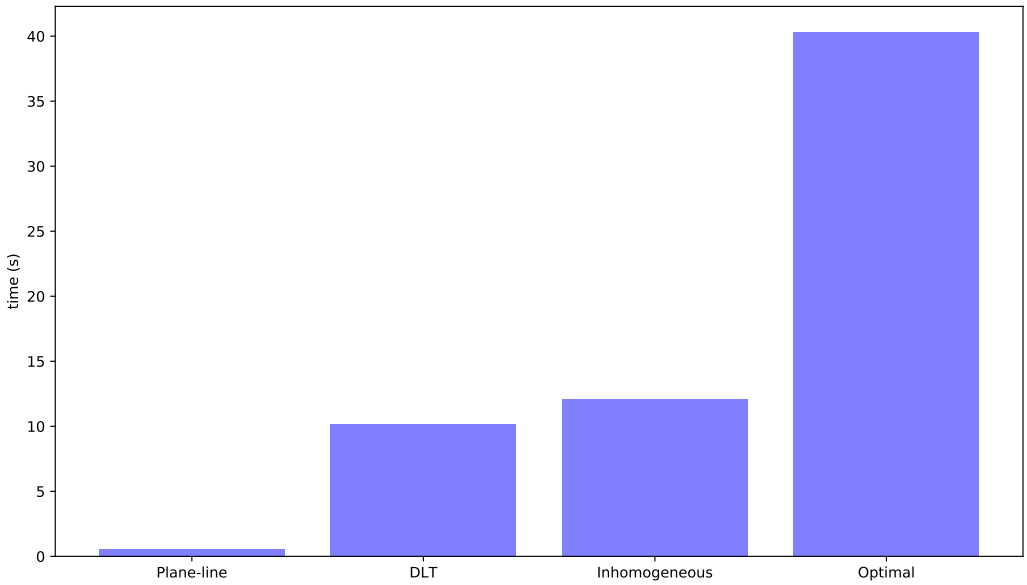

Figure 7. Mean execution time of the methods, reconstructing 1310720 points 10 times.

maximum accuracy that a system can achieve under a given phase-depth sensitivity. Furthermore, the plane-line triangulation method (with lens distortion correction) achieves the same accuracy regardless of how the other projector coordinate is obtained, i.e., through epipolar constraint or by projecting along the other direction. The epipolar constraint may prove useful in high-speed applications, in which a reduced number of projected patterns is desired.

If we manage to arrange an SL system with optimal phase-depth sensitivity, then any triangulation method should yield approximately the same accuracy, which should be considered when designing SL systems. Finally, having ensured an optimal configuration, the plane-line triangulation method with lens distortion correction offers the same accuracy as the other line-line triangulation methods and is the least computationally expensive.

FUNDING

Universidad Tecnológica de Bolívar, MinSalud, and MinCiencias (935-2019).

ACKNOWLEDGMENTS

R. Vargas and J. Meza thank Universidad Tecnológica de Bolívar (UTB) for a post-graduate scholarship, MinCiencias, and MinSalud for a "Joven Talento" scholarship. L.A. Romero and A.G. Marrugo thank UTB for a Research Leave Fellowship, also Sandra Santana, and Johann Vera for their invaluable assistance amidst the current emergency. A.G. Marrugo acknowledges support from the Fulbright Commission in Colombia and the Colombian Ministry of Education within the framework of the Fulbright Visiting Scholar Program, Cohort 2019-2020.

REFERENCES

[1] Zhang, S., [*High-Speed 3D imaging with digital fringe projection techniques*], CRC Press (2018).

[2] Takeda, M. and Mutoh, K., "Fourier transform profilometry for the automatic measurement of 3-d object shapes," *Applied optics* **22**(24), 3977–3982 (1983).

[3] Zhang, S. and Huang, P. S., "Novel method for structured light system calibration," *Optical Engineering* **45**(8), 083601–083601 (2006).

[4] Vargas, R., Marrugo, A. G., Zhang, S., and Romero, L. A., "Hybrid calibration procedure for fringe projection profilometry based on stereo vision and polynomial fitting," *Applied Optics* **59**(13), D163–7 (2020).

[5] Hartley, R. and Zisserman, A., [*Multiple view geometry in computer vision*], Cambridge university press (2003).

[6] Wang, Y. and Zhang, S., "Optimal fringe angle selection for digital fringe projection technique," *Applied optics* **52**(29), 7094–7098 (2013).

[7] Zhou, P., Liu, X., and Zhu, T., "Analysis of the relationship between fringe angle and three-dimensional profilometry system sensitivity," *Applied optics* **53**(13), 2929–2935 (2014).

[8] Zhang, R., Guo, H., and Asundi, A. K., "Geometric analysis of influence of fringe directions on phase sensitivities in fringe projection profilometry," *Applied optics* **55**(27), 7675–7687 (2016).

[9] Vargas, R., Marrugo, A. G., Pineda, J., Meneses, J., and Romero, L. A., "Camera-projector calibration methods with compensation of geometric distortions in fringe projection profilometry: A comparative study," *Opt. Pura Apl* **51**(3), 50305–1 (2018).

[10] Zhang, W., Li, W., Yu, L., Luo, H., Zhao, H., and Xia, H., "Sub-pixel projector calibration method for fringe projection profilometry," *Optics express* **25**(16), 19158–19169 (2017).

[11] Vargas, R., Marrugo, A. G., Pineda, J., Meneses, J., and Romero, L. A., "Evaluating the influence of camera and projector lens distortion in 3d reconstruction quality for fringe projection profilometry," in [*3D Image Acquisition and Display: Technology, Perception and Applications*], 3M3G–5, Optical Society of America (2018).

[12] Yang, T., Zhang, G., Li, H., Zhang, Z., and Zhou, X., "Theoretical proof of parameter optimization for sinusoidal fringe projection profilometry," *Optics and Lasers in Engineering* **123**, 37–44 (2019).

[13] Rao, G., Song, L., Zhang, S., Yang, X., Chen, K., and Xu, J., "Depth-driven variable-frequency sinusoidal fringe pattern for accuracy improvement in fringe projection profilometry," *Optics express* **26**(16), 19986–20008 (2018).

[14] Li, B. and Zhang, S., "Structured light system calibration method with optimal fringe angle," *Applied optics* **53**(33), 7942–7950 (2014).

[15] Nie, L., Ye, Y., and Song, Z., "Method for calibration accuracy improvement of projector-camera-based structured light system," *Optical Engineering* **56**(7), 074101 (2017).